Natural-convective high-temperature oxidation of iridium
by Neil Kelly Wahl

A thesis submitted to the Graduate Faculty in partial fulfillment of the requirements for the degree of
MASTER OF SCIENCE in Mechanical Engineering
Montana State University

Abstract:
An investigation of oxidation of iridium wire in naturally-convected oxygen and air was performed in the temperature range of 1675 to 2260°C (1948 to 2533°K) and the pressure range of 9.8 x 10^-8 to 1.32 atmospheres (7.5 x 10^-5 to 1000 torr). Two theoretical models were developed, each extending over specific pressure ranges. One model described the surface recession rate at low pressures where metal vaporization predominated the rate. The second model described the surface recession rate at high pressures where it was assumed that diffusion of Ir(g), IrO2(g), and IrO3(g) through a gaseous boundary layer controlled the rate. A close correlation between the experimental results and theoretical calculations was achieved for oxidation in both oxygen and air.

Empirical equations that describe the temperature dependence of the free energies of formation of IrO2(g) and Ir03(g) were developed. Results from these equations agree fairly well with results of previous investigators.

Statement of Permission to Copy

In presenting this thesis in partial fulfillment of the requirements for an advanced degree in Mechanical Engineering at Montana State University, I agree that the Library shall make it freely available for inspection. I further agree that permission for extensive copying of this thesis for scholarly purposes may be granted by my major professor, or, in his absence, by the Director of Libraries. It is understood that any copying or publication of this thesis for financial gain shall not be allowed without my written permission.

Signature Neil Kelly Wahl

Date May 24, 1974

NATURAL-CONVECTIVE HIGH-TEMPERATURE OXIDATION OF IRIDIUM

by

NEIL KELLY WAHL

A thesis submitted to the Graduate Faculty in partial fulfillment of the requirements for the degree

of

MASTER OF SCIENCE

in

Mechanical Engineering

Approved:

Dennis O. Blackketter
Head, Major Department

R T Weinberg
Chairman, Examining Committee

Henry L Parsons
Graduate Dean

MONTANA STATE UNIVERSITY
Bozeman, Montana

June, 1974

ACKNOWLEDGMENTS

Special thanks and appreciation are extended to Dr. R. T. Wimber for his guidance and assistance in the research and for serving as head of the associated examining committee. Thanks are also given to Dr. E. H. Bishop and Dr. R. E. Powe for serving as members of the examining committee. Dr. Powe is the author of the extensively used least-squares curvefitting computer program used in this research. The Atomic Energy Commission is also thanked for the financial support of this research.

TABLE OF CONTENTS

LIST OF TABLES

LIST OF FIGURES

NOMENCLATURE

Symbols

A	Equivalent weight equal to 192.2 gms of iridium consumed per gm mole of oxide formed divided by the density of the iridium.
α	Accommodation coefficient
α'	Power used in describing diameter dependencies
α_v	Vaporization coefficient
β	Coefficient of thermal expansion - $(^oK)^{-1}$
C_p	Specific heat at constant pressure of the oxidizing gas - cal/$(gm\,^oK)$
C_v	Specific heat at constant volume of the oxidizing gas - cal/$(gm\,^oK)$
D	Diameter of wire - cm
D_v	Molecular diffusivity - cm^2/sec
ΔF_f^o	Standard-state free energy of formation - kcal/mole
ΔL	Percent thermal expansion of the iridium wire
ΔT	Difference between wire temperature and ambient temperature - ^oK
ϵ_{12}	Energy of molecular interaction - ergs
$\epsilon_1/\bar{k}$	Force constant for oxidizing gas - ^oK
$\epsilon_2/\bar{k}$	Force constant for oxide specie - ^oK
g	Gravitational acceleration - cm/sec^2
γ	Specific heat ratio for the oxidizing gas
Gr	Grashof number
h	Convective heat-transfer coefficient - $cal/(cm^2 sec\,^oK)$

Symbols

I_D	Collision integral for diffusion
J	Flux equal to moles of vapor molecules that leave a surface per unit area and time
k	Thermal conductivity of the oxidizing gas - cal/(cm sec ^oK)
$\bar{k}$	Boltzmann constant - 1.38×10^{-6} ergs/^oK
K	Equilibrium constant
k_G	Gas-film mass transfer coefficient for diffusion of oxide specie through the boundary layer - gm mole/(sec cm^2 atm)
λ	Mean free path of gas molecules - cm
M	Molecular weight of the oxidizing gas
M_i	Molecular weight of the diffusing oxide specie
μ	Viscosity of the oxidizing gas - gm/(cm sec)
Nu	Nusselt number
P	Total pressure - atm
P_{BM}	Logarithmic mean pressure of nondiffusing oxygen - atm
P_{eq}	Equilibrium pressure of the vaporizing specie - atm
P_i	Partial pressure of the i^{th} specie - atm
P_{O_2}	Partial pressure of oxygen - atm
P_M	Partial pressure of the iridium metal - atm
Pr	Prandtl number
R	Ideal gas constant - 1.987 cal/(gm mole ^oK) or 82.06 cm^3 atm/(gm mole ^oK)
$(r_o)_1$	Collision diameter for collision between oxidizing gas molecules - angstroms

Symbols

$(r_o)_2$	Collision diameter for collision between molecules of iridium containing species - angstroms
r_{12}	Collision diameter for collision between oxygen molecule and molecule of iridium containing species - angstroms
Ra	Rayleigh number
ρ	Density of the oxidizing gas - gm/cm^3
$\rho_{Ir,\ T_k}$	Density of iridium at T_k - gm/cm^3
T_f	Film temperature - ^oK
T_k	Wire temperature - ^oK
T_M	Melting temperature for oxides - ^oK
$(V_o)_1$	Molal volume of oxidizing gas - cm^3(gm mole)
$(V_o)_2$	Molal volume of the oxide specie - cm^3(gm mole)
$\dot{x}$	Surface recession rate - cm/sec
$\dot{x}_s$	Standardized recession rate - cm/sec

ABSTRACT

An investigation of oxidation of iridium wire in naturally-convected oxygen and air was performed in the temperature range of 1675 to 2260°C (1948 to 2533°K) and the pressure range of 9.8×10^{-8} to 1.32 atmospheres (7.5×10^{-5} to 1000 torr). Two theoretical models were developed, each extending over specific pressure ranges. One model described the surface recession rate at low pressures where metal vaporization predominated the rate. The second model described the surface recession rate at high pressures where it was assumed that diffusion of Ir(g), $IrO_2(g)$, and $IrO_3(g)$ through a gaseous boundary layer controlled the rate. A close correlation between the experimental results and theoretical calculations was achieved for oxidation in both oxygen and air.

Empirical equations that describe the temperature dependence of the free energies of formation of $IrO_2(g)$ and $IrO_3(g)$ were developed. Results from these equations agree fairly well with results of previous investigators.

CHAPTER I

INTRODUCTION

Characteristics and Uses of Iridium

Iridium, the 77^{th} element, is a platinum group metal. It is the only elemental metal known to man that possesses a low enough oxidation rate and a high enough melting point, 2454°C (2727°K), that it can be used unprotected in an oxygen containing gas for extended periods of time at temperatures greater than 2000°C. At temperatures greater than 1000°C, iridium forms volatile oxides and a bare surface is left behind. This results in oxidation rates that are linear with time.

When compared to other metals, iridium is one of the most corrosion resistant over a wide range of temperatures and corrosive environments. The corrosive environments included various acids, salt solutions, fused salts, molten metals, and molten metal oxides.

Iridium has been used as heating elements in high temperature furnaces, standardized high-temperature thermocouples, and for protective coatings of less expensive materials such as tungsten and tantalum base alloys. Potential applications for iridium are leading edges of reentry space vehicles, reactor components, and parts in rockets and turbine engines.

Iridium also has limitations. Being a platinum group metal, the cost of iridium could be a factor restricting extensive use. Weight could be another constraint. Iridium is one of the most dense (22.57 gm/cm^3) elements known to man. The very low emittance of iridium could

restrict its use as leading edges for reentry vehicles. The primary means of heat dissipation from the leading edge is radiation. The low emittance would then restrict the heat dissipation. The emittance of iridium can be enhanced by oxide overcoats and would not present serious problems to the use as a leading edge material.

Review of Prior Work

The brief review of past work done on the oxidation of iridium contained in the following resulted in conclusions used as a starting point for the present studies.

Several separate investigators have studied the products of the oxidation of iridium and the thermodynamics involved in the formation of these products. Cordefunke and Meyer (1) studied the oxidation of iridium in the temperature range of 1169 to 1462°C (1442 to 1735°K). They concluded that $IrO_3(g)$ was the major specie formed. Their results were confirmed by other workers (2,3).

Mass spectrometric studies by Norman et al (4) resulted in their conclusion that $IrO_2(g)$ and $IrO_3(g)$ were the major species of oxidation. The presence of $IrO(g)$ could not be ruled out completely. If $IrO(g)$ was present, its partial pressure was estimated to be less than 2 percent of the partial pressure of $IrO_2(g)$ at the highest temperature investigated. The work of Norman et al involved feeding oxygen at 10^{-4} atm into an iridium Knudsen cell heated to 1557 - 1760°C (1830 - 2033°K). Standard-state enthalpies and entropies of formation for $IrO_2(g)$ were reported as 48.5

$\pm$ 0.8 kcal/mole and 3.9 $\pm$ 2.0 eu respectively. The standard-state enthalpies and entropies of formation for $IrO_3(g)$ were reported as 5.5 $\pm$ 1.5 kcal/mole and -13.1 $\pm$ 2.5 eu respectively.

Studies performed by Olivei (5) resulted in the conclusions that $IrO_2(g)$ and $IrO_3(g)$ were the major species formed. This work was done over the pressure range of 10^{-8} to 10^{-10} atm and over the temperature range of 880 to 1780°C (1153 - 2053°K). Mass spectrometric studies in the temperature range of 627 to 2227°C (900 - 2500°K) yielded standard-state enthalpy and entropy of formation for $IrO_3(g)$ of 6.0 kcal/mole and -9.5 eu respectively.

Wimber and Kraus (6) concluded that Ir(g) was an important specie at high temperatures and that IrO(g) contributed very little to the overall recession rate.

Based upon the conclusions of these investigators, the iridium containing species that significantly contributed to the oxidation rate were thought to be Ir(g), $IrO_2(g)$, and $IrO_3(g)$.

CHAPTER II

EXPERIMENTAL EQUIPMENT AND PROCEDURES

Experimental Materials

Commercially pure iridium wire was purchased in three lots. Results of mass spectrometric and emission spectrographic analyses along with an indication of the sources and wire diameters are given in Table 1. The major impurity in Lots 1 and 2 was tungsten at 0.6 percent and 0.071 percent respectively. The major impurities in Lot 3 were tungsten (0.02%) and barium (0.02%). The analyses did not include all known elements, but the iridium content was estimated to be 99.3, 99.9, and 99.9 percent in Lots 1, 2, and 3 respectively.

The oxygen used in the present studies was USP grade. Nitrogen and argon were the major impurities and were assumed to be inert to iridium. The oxygen content was typically 99.7 percent.

The air used in the present studies was atmospheric and was assumed to have an oxygen content of 21 percent (based upon a volume percent).

Experimental Apparatus and Procedure

The equipment used in the present study is shown schematically in Figure 1. An iridium wire specimen 5.6 cm long was mounted horizontally between two electrodes in a cell. The cell, which had water-cooled copper walls, had the internal dimensions of 2.5 x 7.6 x 8.9 cm. The cell was provided with two sight ports containing rotatable optical-quality pyrex windows. Through one window, a timer-actuated camera fitted with a

Table 1. Analysis* of Iridium Wire

Impurity	Lot #1 +	Lot #2 ‡	Lot #3 ‡
Pt	19	<0.5	<30
Rh	20	38.0	<50
Pd	10	11.5	<10
Ru	166	1.5	<50
Au	<1	<0.5	10
Ag	50	<0.5	<10
Pb	<5	<0.5	<30
Sn	5	<0.5	<10
Zn	<10	0.41	<300
Fe	170	64	30
Cu	96	17	<10
Si	43	6.1	10
Mg	41	1.1	<10
Ca	78	0.61	<50
Al	14	35	<10
Ni	10	1.1	<10
Cr	31	0.84	<10
Mn	10	0.69	<10
Sb	<10	<0.5	<500
B	<50	0.0032	<10
Co	10	1.8	<10
As	<10	0.066	<300
Bi	<1	<0.5	<10
Cd	<5	<0.5	<300
W	6000	710	200
N	50	0.24	-
H	4	-	-
O	70	8.3	-
Ta	-	46	<500
In	-	0.26	<10
Zr	-	1.1	<10
Ga	-	0.20	<10
V	-	0.096	<10
Ti	-	0.49	<10
K	-	0.67	-
Cl	-	0.59	-
S	-	0.57	-

Table 1 (continued)

Impurity	Lot #1 +	Lot #2 ‡	Lot #3 ‡
P	-	0.81	-
Na	-	2.2	-
F	-	0.27	-
C	-	15.0	-
Li	-	0.00072	-
Ba	-	0.5	200

* Impurity contents expressed in parts per million.

\+ 25 mil diameter wire drawn by Englehard Industries, Carteret, New Jersey.

‡ 20 mil diameter wire drawn by Johnson, Matthey & Co., London, England.

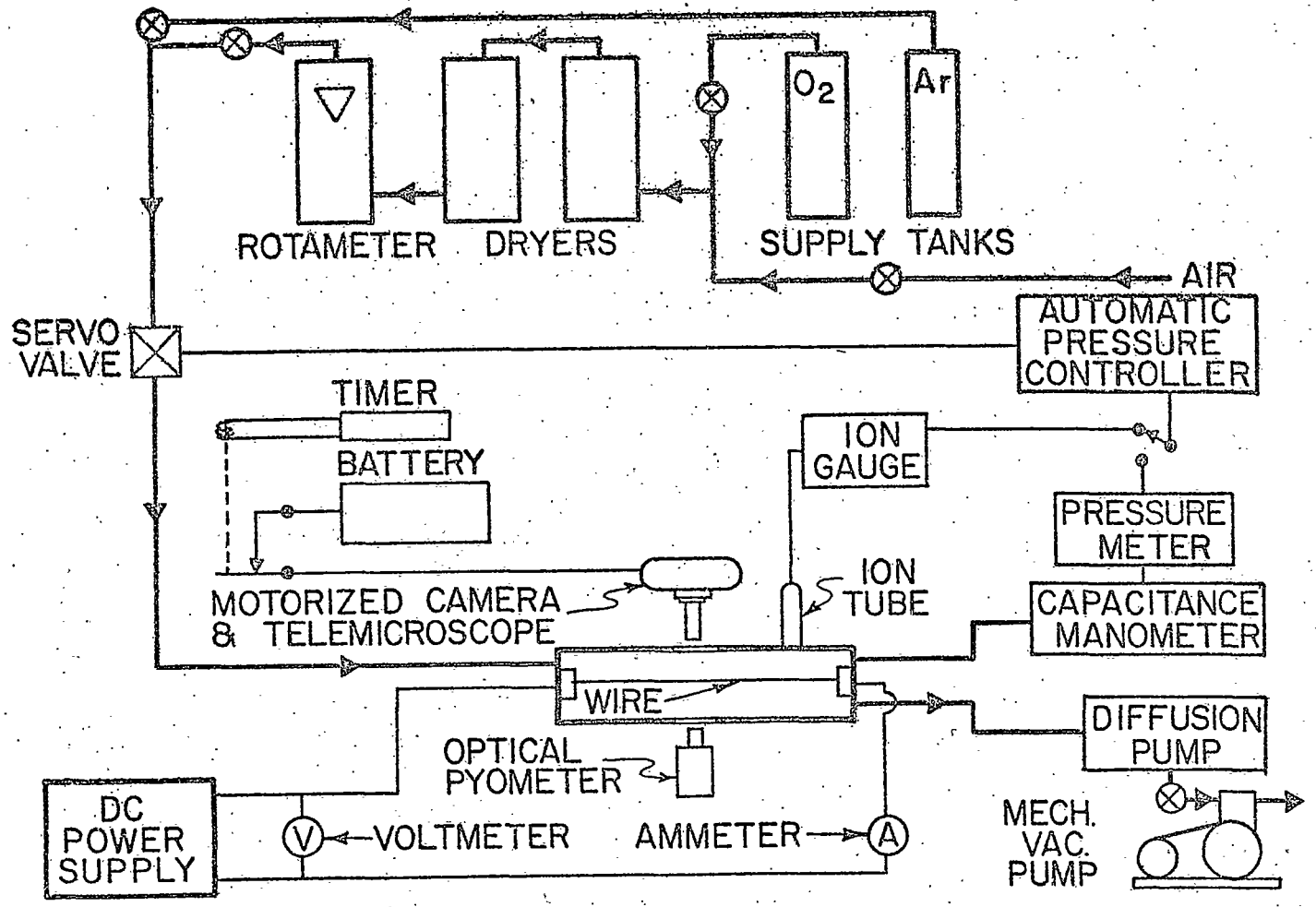

Figure 1. Schematic of Experimental Apparatus

telemicroscope, was used to record the wire diameter at 20x magnification. Through the other window, a Leeds and Northrup 8636-C optical pyrometer equipped with a 38-mm focal length lens was used to determine the brightness temperature of the wire. Errors in temperature measurement would have been caused by condensation of oxides on the windows, but were eliminated by rotating the window to a clean section only when a temperature measurement was being made. The window on the camera side was rotated to a clean section immediately before a picture was taken and immediately after the picture, returned to the original position. The windows were cleaned and polished between runs.

The oxidation cell was mounted on top of a vertical cylinder 10 cm in diameter and 20 cm long. Oxidizing gas was introduced into the cylinder at a point 10 cm below the cell. Through one pressure tap, located 5 cm above and rotated 90° from the gas inlet, an ion tube was used to measure low pressures. Through a second pressure tap, located 5 cm below and rotated 90° from the gas inlet, a capacitive manometer was used to measure high pressures.

Immediately below the cylinder was mounted a water-cooled optically-dense baffle. A Varian/NRC Model M-4 (800 liter/sec) diffusion pump was mounted below the baffle. The baffle prevented a direct line of sight of the pump oil from the pump into the oxidation cell. By means of a hose and tubing, the outlet of the diffusion pump was connected to the inlet of a mechanical pump.

Pressures in the system that were less than 1.32×10^{-4} atm (0.10 torr) were measured with a Westinghouse ion tube (part number WL 7903) and Granville-Phillips Ionization Gauge Controller (series 224) system. Pressures in the system that were greater than or equal to 1.32×10^{-4} atm (0.10 torr) were measured with a MKS Capacitance Manometer 77H-1000 and a MKS Baratron TM Type 77 Pressure Meter. A signal from the measuring instrument was used as an input signal for a Granville-Phillips Automatic Pressure Controller (APC) No. 0-00-216006. The APC operated a servo-driven valve and thus regulated the flow of the oxidizing gas into the system. Before entering the system, the oxidizing gas passed through two driers (the first contained calcium sulfate hemihydrate and the second contained anhydrous magnesium perchlorate) and then through a Matheson No. 74 rotameter.

Current from a Hewlett Packard D.C. Power Supply 6260B was used to self-resistance heat the iridium wire specimen. The voltage across the cell was measured with a Honeywell Digitest Multimeter Model 333R. Current through the wire was measured with a General Electric D.C. Ammeter with a capacity of 50 amperes. The thermal expansion of the wire was accommodated by a cantilever spring arrangement on one of the electrodes. The wire was prestressed to an amount such that when the wire was at the oxidation temperature it was at near zero stress.

Prior to making a run, the wire was cleansed in acetone, mounted between the electrodes, and given an anneal for thirty minutes at 2260°C (2533°K) in an argon atmosphere. The purpose of the anneal was to elim-

inate recrystallization and grain growth during oxidation and to attain an electrical resistivity nearly constant with time. This anneal was given only to each new section of wire. After the anneal, the system was evacuated and then backfilled with the desired oxidizing gas. The system was again evacuated, leak-checked, and refilled with the oxidizing gas to the desired pressure level. Once the pressure stabilized, the iridium wire specimen was brought up to the oxidation temperature by slowly increasing the current through the wire. Once the temperature had stabilized, a series of ten film exposures were made at a predetermined time interval. The time interval was selected such that approximately 0.0254 mm (1 mil) was removed from the diameter of the wire during the total time of the run. The film was then removed, developed, and allowed to dry for a minimum of 2 hours before the images of the wire were measured. The images were measured by an instrument that consisted of a modified cathetometer, high intensity light source, and a Gossen Luna-Pro Exposure Meter. The telemicroscope of the cathetometer was modified to include a 0.05 mm (2 mil) slit at the reticle plane. Each frame was measured at three locations (the two ends and the center of the image). The average diameter was converted to an actual diameter by using a conversion factor. The conversion factor was obtained from the measurement of an image of a reference rod of 0.0655 cm (25.8 mil) in diameter. The repeatability of a single diameter measurement was $\pm$ 0.05 to 0.1 percent. Asymmetry of the wire was determined by Wimber and Kraus (6) to always be less than 1.2 percent.

CHAPTER III

TRUE WIRE TEMPERATURE DETERMINATIONS

A thermocouple technique used by Halvorson and Wimber (7) to determine the relationship between measured pyrometer temperature and true wire temperature was modified based upon the work of McLaren et al (8). The technique used in the present studies consisted of fusion welding each of the leads of an Ir-Ir40Rh thermocouple to an iridium wire specimen which was mounted between the electrodes of the cell. The specimen was self-resistance heated by an AC power supply. An R-C filtering circuit was used to block the AC voltage from the digital millivoltmeter which was used to measure the thermocouple emf. The thermocouple output was taken as an indication of the true wire temperature at the point where the Ir40Rh lead of the thermocouple was attached to the specimen. This point is also the location where the specimen temperature was measured with an optical pyrometer.

Table 2 contains a summary of the pyrometer temperatures measured through a window and the corresponding true wire temperature for wire heated in oxygen or air.

Table 2. Results of True Wire Temperature Determinations

Pyrometer Temperature*, °C (K)		True Wire Temperature, °C (K)	
1500	(1773)	1675	(1948)
1615	(1888)	1820	(2093)
1730	(1903)	1965	(2238)
1850	(2123)	2110	(2383)
1965	(2238)	2260	(2533)

* Measured through a 3/16 inch thick shadowgraph-grade, optical-quality pyrex window.

CHAPTER IV

EXPERIMENTAL RESULTS

Figure 2 consists of a plot of the diameter measurements versus time for a typical run. The surface recession rate is calculated by dividing the slope of the straight line by minus two. Figure 3 contains the measured surface recession rates at temperatures in the range of 1675 to 2260 ^{o}C (1948 to 2533^{o}K) and over the pressure range of 9.8×10^{-8} to 1.32 atmospheres (7.5×10^{-5} to 1000 torr) for oxidation in oxygen. For sake of clarity not all the results are shown. Figure 4 contains the measured surface recession rates in the temperature range of 1675 to 2260^{o}C (1948 to 2533^{o}K) and over the pressure range of 9.8×10^{-8} to 0.66 atmospheres (7.5×10^{-5} to 500 torr) for oxidation in air.

Table 10 in the appendix contains a summary of experimental conditions and recession rates for work done in oxygen by Kraus (9) and the present investigator. Table 11 in the appendix contains a summary of these same parameters for work done in air by this investigator.

Analysis of either the Figures 3 and 4 or the Tables 10 and 11 in the appendix revealed no apparent difference in the oxidation behavior of the various lots of wire.

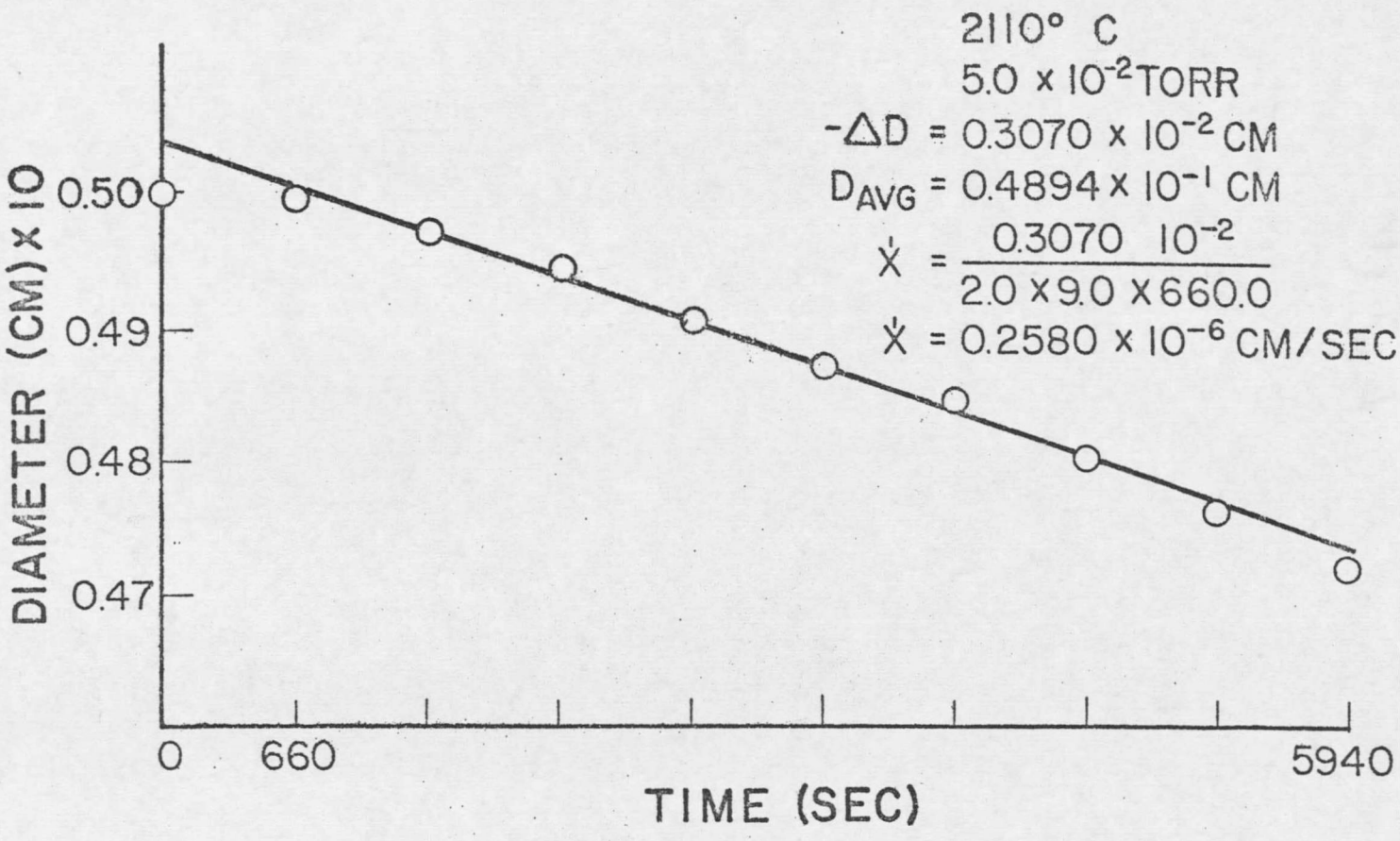

Figure 2. Example of a Rate Graph

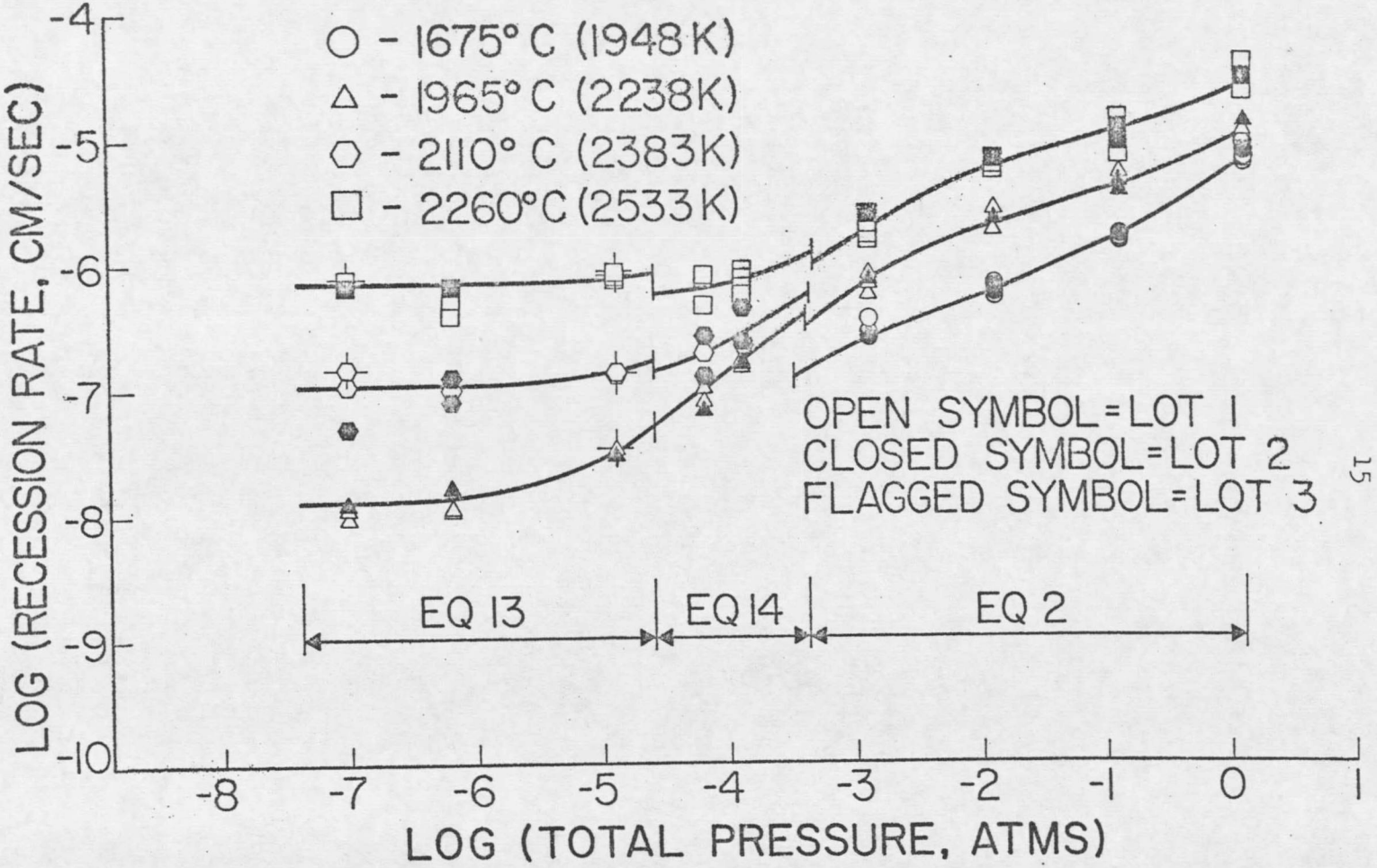

Figure 3. Experimental Results and Theoretical Correlation for Oxidation in Oxygen

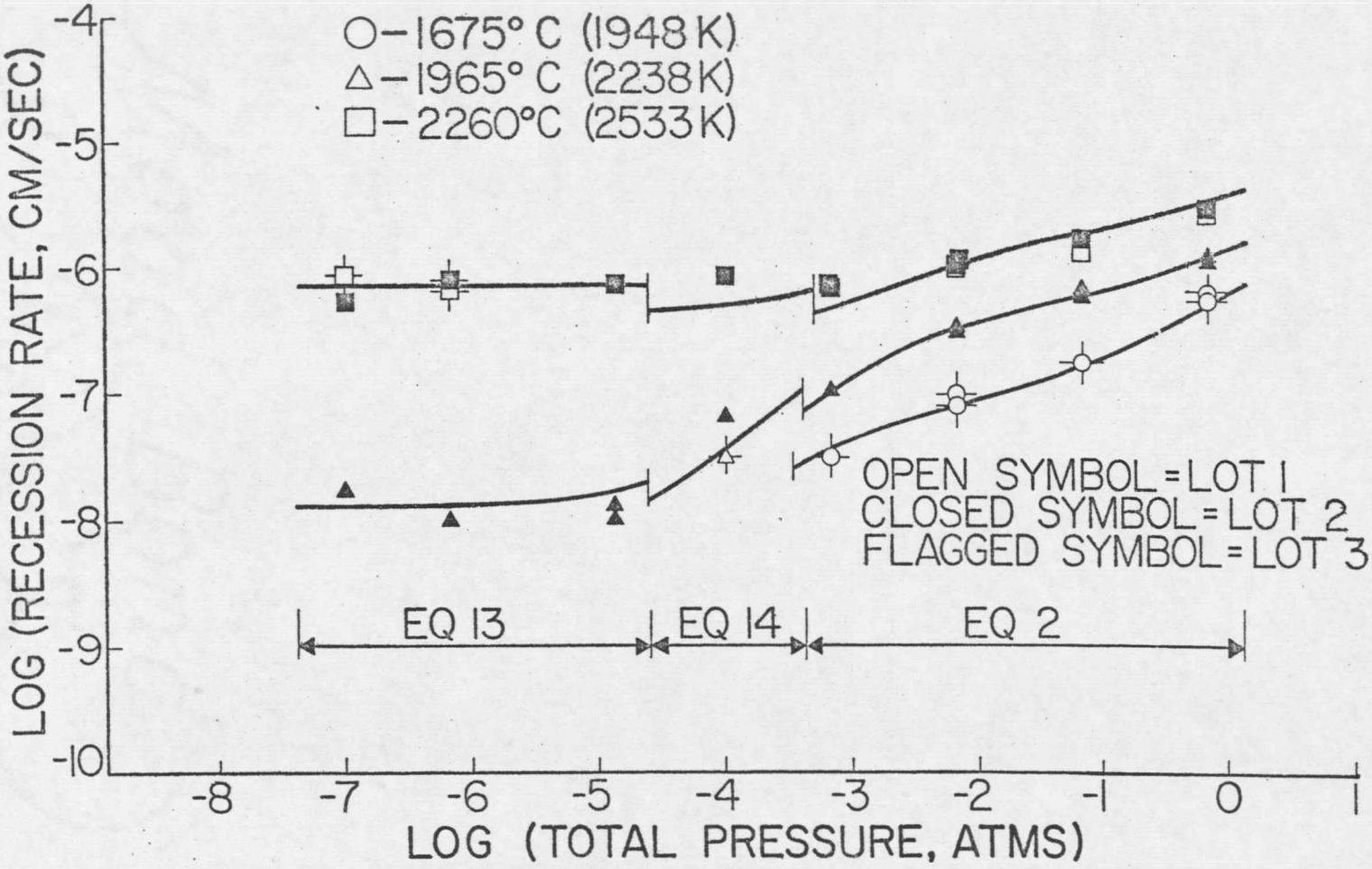

Figure 4. Experimental Results and Theoretical Correlation for Oxidation in Air

CHAPTER V

THEORETICAL RATE CALCULATIONS

The theoretical surface recession rates were calculated from three different equations. Each equation was valid over a specific pressure range. The three pressure ranges were high pressures ($P \geq 4 \times 10^{-4}$ atm), low pressures ($P \leq 3 \times 10^{-5}$ atm), and intermediate pressures ($3 \times 10^{-5} < P < 4 \times 10^{-4}$ atm).

Theoretical Rates at High Pressures

At high pressures ($P \geq 4 \times 10^{-4}$ atm), where a boundary layer is present, the oxidation rate was found to be best described as being controlled by diffusion of the iridium-containing species through the boundary layer (6). The consumption of the iridium metal is equal to the total flux of iridium-containing species and thus the oxidation rate, expressed as a surface recession rate, is represented by the following equation:

$$\dot{x} = \sum_i A \, k_{Gi} \, P_i \qquad [1]$$

where A is an equivalent weight (mass of iridium consumed per mole of diffusing specie formed) divided by the density of iridium, k_{Gi} is the mass transfer coefficient for the i^{th} specie, P_i is the partial pressure of the i^{th} specie at the inner surface of the boundary layer, and $\dot{x}$ is the surface recession rate.

The partial pressures of the different species at the inner surface of the boundary layer can be calculated from the respective equilibrium constants (treated as unknowns) and the oxygen partial pressure. Equation

1, then, becomes:

$$\dot{x} = A(k_{G2} K_2 P_{O_2} + k_{G3} K_3 P_{O_2}^{3/2} + k_{GM} P_M) \qquad [2]$$

where K_2 is the equilibrium constant for the formation of $IrO_2(g)$, K_3 is the equilibrium constant for the formation of $IrO_3(g)$, P_M is the vapor pressure of the iridium metal at the inner surface of the boundary layer, and P_{O_2} is the partial pressure of oxygen.

The partial pressure of iridium metal can be calculated from the empirical vapor pressure equation of Honig and Kramer (10):

$$\log(760\ P_M) = -8464.67/T_k + 65.5812 \log(T_k) - 0.0100272\ T_k + 5.44981 \times 10^{-7}\ T_k^2 \qquad [3]$$

where P_M is the vapor pressure of the metal in atmospheres and T_k is the temperature of the wire in ^oK.

The mass transfer coefficients can be calculated from an expression which was obtained from the Chilton-Colburn equations (11)

$$k_{Gi} = \frac{h\ P}{R\ T_f\ C_p\ \rho\ P_{BM}} \left(\frac{C_p\ \rho\ D_{vi}}{k} \right)^{2/3} \qquad [4]$$

where h is the convective heat-transfer coefficient, P is the total pressure, R is the ideal gas constant, T_f is the film temperature (the arithmetic mean of the wire temperature and the ambient temperature), C_p is the specific heat of the oxidizing gas at constant pressure, ρ is the density

of the oxidizing gas, P_{BM} is the logarithmic mean pressure of the nondiffusing oxidizing gas (thus, $P_{BM} \approx P$), k is the thermoconductivity of the oxidizing gas, and D_{vi} is the gaseous diffusivity for the i^{th} specie.

The properties for the two oxidizing gases were least-squares curve-fit over a film-temperature range of 1000°K to 1400°K for original data (12,13). Tables 3 and 4 contain the resulting equations and an indication of the effectiveness of the fit. The mean free path equations for each gas were developed from the Dushman equation (14).

The convective heat-transfer coefficient was evaluated from two different equations for the Nusselt number, the Madden-Piret (15) equation and the Drake et al (16) equation. In subsequent computer calculations, it was found that the Madden-Piret equation yielded a slightly better correlation between calculated and experimental recession rates.

The Madden-Piret equation for the Nusselt number is:

$$Nu = \frac{2}{\ln(6.82/Ra^{1/3}) + 8k\lambda/\alpha(\gamma + 1)\mu C_v D - \ln(1 + 2\lambda/D)}$$

$$= \frac{h D}{k}$$

where λ is the mean free path in the gas, D is the diameter of the wire, α is the thermal accommodation coefficient (treated as an unknown), C_v is the specific heat at constant volume for the oxidizing gas, and Ra is the dimensionless Rayleigh number. The Rayleigh number is the product of the Grashof and Prandtl numbers:

Table 3. Properties of Air

$1000^{\circ}K \leq T_f \leq 1400^{\circ}K$

Property	Relation	Max. % Deviation
Density (gm/cm^3)	$\rho = 0.3530\ P/T_f$	0.011
Specific Heat ($cal/gm/^{\circ}K$)	$C_p = 0.0773\ T_f^{0.1825}$	0.082
Viscosity ($gm/sec/cm$)	$\mu = 7.313 \times 10^{-6}\ T_f^{0.5849}$	0.081
Thermal Conductivity ($cal/cm/sec/^{\circ}K$)	$k = 1.239 \times 10^{-6}\ T_f^{0.7023}$	0.31
Specific Heat Ratio (dimensionless)	$\gamma = 2.001\ T_f^{-0.0585}$	0.018
Mean Free Path (cm)	$\lambda = 1.5347 \times 10^{-8}\ \frac{T_f^{1.0849}}{P}$	-

NOTE: P is the total pressure in atmospheres.

T_f is the film temperature in $^{\circ}K$.

Table 4. Properties of Oxygen

$1000^{\circ}K \leq T_f \leq 1400^{\circ}K$

Property	Relation	Max. % Deviation
Density (gm/cm^3)	$\rho = 0.3899\ P/T_f$	0.04
Specific Heat ($cal/gm/^{\circ}K$)	$c_p = 0.116\ T_f^{0.117}$	0.21
Viscosity ($gm/sec/cm$)	$\mu = 5.374 \times 10^{-6}\ T_f^{0.650}$	0.44
Thermal Conductivity ($cal/cm/sec/^{\circ}K$)	$k = 8.12 \times 10^{-7}\ T_f^{0.7738}$	0.65
Specific Heat Ratio (dimensionless)	$\gamma = 1.682\ T_f^{-0.0359}$	0.08
Mean Free Path (cm)	$\lambda = 1.074 \times 10^{-8}\ \frac{T_f^{1.15}}{P}$	-

NOTE: P is the total pressure in atmospheres.

T_f is the film temperature in $^{\circ}K$.

$$Ra = Gr\ Pr$$

$$= (g \rho^2 D^3 \beta \Delta T/\mu^2)(C_p \mu/k) \qquad [6]$$

where g is the acceleration of gravity, β is the coefficient of thermal expansion for the oxidizing gas, and ΔT is the difference between the wire temperature and the ambient temperature.

D_{vi}, the gaseous diffusivity, was calculated from the Wilke-Lee modified Hirschfelder-Bird-Spotz equation (17):

$$D_{vi} = \frac{[10.7 - 2.46(1/M_i + 1/M)^{1/2}]\ 10^{-4}\ T_f^{3/2}(1/M_i + 1/M)^{1/2}}{P\ r_{12}^2\ I_D} \qquad [7]$$

where

M_i is the molecular weight of the i^{th} diffusing specie,

M is the molecular weight of the oxidizing gas,

$r_{12} = \frac{(r_o)_1 + (r_o)_2}{2}$, the collision diameter for collision between the oxidizing gas molecule and the molecule of an iridium containing specie,

$(r_o)_1 = 1.18(V_o)_1^{1/3}$, collision diameter for collision between oxidizing gas molecules,

$(r_o)_2 = 1.18(V_o)_2^{1/3}$, collision diameter for collision between molecules of an iridium containing specie,

$(V_o)_1$ is the molal volume of the oxidizing gas,

$(V_o)_2$ is the molal volume of the iridium containing specie,

I_D = $0.673(\bar{k}\ T_f/\epsilon_{12})^{-0.324}$, collision integral for diffusion (result of a least-squares curvefit of original data (9)),

ϵ_{12} is the energy of molecular interaction,

$\bar{k}$ is the Boltzmann constant (1.38×10^{-6} ergs/^oK).

The value of ϵ_{12} was calculated from the equation:

$$\epsilon_{12}/\bar{k} = ((\epsilon_1/\bar{k})(\epsilon_2/\bar{k}))^{1/2}$$

where $\epsilon_1/\bar{k}$ is known for the oxidizing gas (for O_2 = 113.2^oK, for air = 97.0 ^oK) and $\epsilon_2/\bar{k}$ was determined for the different diffusing species from the relation:

$$\epsilon_2/\bar{k} = 1.92\ T_m$$

T_m is the melting temperature of the oxides, treated as an unknown in this analysis (but known to be greater than 1383^oK for IrO_2 (18,19)).

The coefficient, A, of Equation 2 was calculated from the equation:

$$A = \frac{192.2 \text{ gm Ir consumed/mole diffusing specie formed}}{\rho_{Ir,\ T_k}}$$

where

$$\rho_{Ir,\ T_k} = \frac{\rho_{Ir,\ 298^oK}}{(1 + \Delta L_{T_k}/100)^3} \qquad [8]$$

ΔL, the percent linear thermal expansion, was calculated from the equation:

$$\Delta L_{T_k} = 6.144 \times 10^{-6} T_k^{1.632}$$

which was the result of curvefitting the thermal-expansivity results of Halvorson and Wimber (7).

A successive-substitution computer method was used to determine the optimum values of each of the unknowns, α, K_2, K_3, and T_m, for the experimental results of oxidation. This was done only for the results in oxygen at high pressures. From this method, it was found that oxide-melting temperatures in the range of 1400 to 1800°K had very little effect on the results. As a melting temperature of 1400°K did yield very slightly better results, it was chosen as the oxide melting temperatures.

The accommodation coefficient and the equilibrium constants were functions of wire temperature. The optimum values of the accommodation coefficient were least-squares curvefit over the temperature range of 1948 to 2533°K. The resulting equation for α was:

$$\alpha = 335.631 - 0.488564\ T_k + 2.55837 \times 10^{-4}\ T_k^2 - 5.57098 \times 10^{-6}\ T_k^3 + 4.03322 \times 10^{-12}\ T_k^4 \qquad [9]$$

(maximum deviation of the equation from optimum values was 0.000249%). The free energies of formation were calculated from the equilibrium constants by using the equation:

$$\Delta F_f^{\circ} = (-R\ T_k\ \ln K)/1000$$

where ΔF_f° is the free energy of formation, R is the ideal gas constant,

T_k is the absolute wire temperature, and K is the equilibrium constant. Values of the free energies of formation obtained from the equilibrium constants were also least-squares curvefit over the temperature range of 1948 to 2533°K. The resulting equations were:

$$\Delta F_f^{\circ}[IrO_2(g)] = 541.458 - 0.668736\ T_k + 2.91610 \times 10^{-4}\ T_k^2 - 4.27297 \times 10^{-8}\ T_k^3,\ \text{kcal/mole} \qquad [10]$$

(maximum deviation was 0.26%), and

$$\Delta F_f^{\circ}[IrO_3(g)] = 214.180 - 0.298810\ T_k + 1.49832 \times 10^{-4}\ T_k^2 - 2.41895 \times 10^{-8}\ T_k^3,\ \text{kcal/mole} \qquad [11]$$

(maximum deviation was 0.27%).

These empirical equations were used in the calculation of surface recession rates for oxidation in oxygen. Numerical values for the calculated rates at the experimental conditions are presented in Table 10 in the appendix. Recession rates calculated from Equation 2 for a wire 0.0559 cm in diameter are represented by curves shown in Figure 3.

The degree of correlation between the experimental and calculated rates is shown in Table 5. To perform this analysis, the necessity to develop a method that would "standardize" the rates to a common diameter arose. This was necessary as the experimental and calculated rates are dependent upon the wire diameter. The diameter dependency was found to be described by raising the diameter of the wire to a power (result of least-squares curve-

Table 5. Effectiveness of the Final Correlation for Rates in Oxygen at Pressures Greater Than 4×10^{-4} atm.

Temp °C	Approximate Experimental Scatter, %	Correlation Disparity, %
1675	5.3	6.8
1820	4.4	4.3
1965	5.1	7.7
2110	9.3	8.0
2260	12.4	13.2
Overall	7.4	8.4

fit of data by Kraus (9)). Table 6 contains a summary of the powers and the respective temperatures.

Table 6. Exponent of Diameter Used in Determining the Diameter Dependency

Wire Temp °C	Exponent of Diameter α'
1675	-0.70
1820	-1.11 *
1965	-1.26
2110	-1.11 *
2260	-1.17

* Estimated values

The wire diameter chosen to represent the standardized value was 0.0559 cm (an average wire diameter). To clarify the calculations made in determining a standardized rate, the following equation may be referred to:

$$\dot{x}_s = \dot{x}(D/0.0559)^{-\alpha'}$$

where $\dot{x}_s$ is the standardized rate, $\dot{x}$ is the actual rate for a wire diameter D, and α' is the appropriate power from Table 6.

The "approximate experimental scatter" is the average absolute deviation of the standardized rates from the mean at a given temperature and pressure. The "correlation disparity" is the average absolute difference between actual experimental rates and rates calculated from Equation 2 (using experimental temperatures, pressures and diameters).

Recession rates in air were calculated using the same equations (with the appropriate equations representing the properties of air and the partial pressure of oxygen). Numerical results for these calculations are presented in Table 11 in the appendix. Figure 4 shows a curve representing the recession rates of a wire 0.0559 cm in diameter calculated from Equation 2.

Limitations on the ranges of validity for these equations are dependent upon the range of validity for the Chilton-Colburn equation (Equation 4) and the Madden-Piret equation (Equation 5). Equation 4 is valid for Prandtl numbers in the range of 0.6 to 100 and for Schmidt numbers $(\mu/\rho D_{vi})$ in the range of 0.6 to 2500. Equation 5 is valid for Rayleigh numbers in the range of 10^{-8} to 10^{-1}. The Prandtl, Schmidt, and Rayleigh numbers in the present study were in the ranges of 0.731 to 0.732, 1.51 to 1.90, and 4.98×10^{-8} to 1.9×10^{-1} respectively.

Theoretical Rates at Low Pressures

At low pressures ($P \leq 3 \times 10^{-5}$ atm), the rate was assumed to be controlled by the vaporization of the iridium-containing species. The flux (moles of vapor molecules that leave a surface per unit area and time) can be calculated from the Hertz-Langmuir equation as modified by Knudsen (20):

$$J = \alpha_v P_{eq} (2\pi M R T_k)^{-1/2}$$

where J is the flux, α_v is the vaporization coefficient (in the present studies assumed equal to one), P_{eq} is the equilibrium pressure of the specie,

M is the molecular weight of the specie, R is the ideal gas constant, and T_k is the absolute temperature of the wire. P_{eq} for the oxides $IrO_2(g)$ and $IrO_3(g)$ can be calculated from the respective equilibrium constant and the partial pressure of oxygen. The equilibrium constants in turn can be calculated from the free energies of formation (Equations 10 and 11). The vapor pressure of the iridium can be calculated from Equation 3.

A surface recession rate is expressed by:

$$\dot{x} = \sum_i \frac{J_i}{\rho_{Ir,\ T_k}} \qquad [12]$$

where J_i is the flux of the i^{th} specie and $\rho_{Ir,\ T_k}$ is the density of iridium at the temperature T_k (calculated from Equation 8). Equation 12 was reduced to the form:

$$\dot{x} = 44.3[P_m(192.2/T_k)^{1/2} + 0.8573\ K_2\ P_{O_2}(224.2/T_k)^{1/2} + 0.8002\ K_3\ P_{O_2}^{1.5}(240.2/T_k)^{1/2}]/\rho_{Ir,\ T_k} \qquad [13]$$

Where $\dot{x}$ is the surface recession rate, P_m is the vapor pressure of the iridium metal, T_k is the absolute wire temperature, K_2 is the equilibrium constant for $IrO_2(g)$, K_3 is the equilibrium constant for $IrO_3(g)$, and P_{O_2} is the partial pressure of oxygen.

A simple computer program was used to calculate recession rates at the experimental conditions, both in oxygen and in air. The results are presented in Tables 10 and 11 in the appendix respectively. The results for both oxygen and air are shown graphically in Figures 3 and 4 respectively.

The degree of correlation between the experimental and calculated rates in oxygen is indicated in Table 7.

Table 7. Effectiveness of the Final Correlation for Rates in Oxygen at Pressures Less Than 3×10^{-5} atm.

Temp °C	Experimental Scatter, %	Correlation Disparity, %
1965	10.0	12.0
2110	16.9	17.3
2260	18.9	21.6
Overall	15.5	17.3

The "experimental scatter" is the average absolute deviation of the experimental recession rate from the mean at a given temperature and pressure.

Limitations on the range of validity for these calculations depends upon the range of validity for Equation 13. Equation 13 is valid for pressures less than 3×10^{-5} atm (based upon a Knudsen number of 5 (21)).

Theoretical Rate Calculations at Intermediate Pressures

The oxidation rates in the intermediate pressure range ($3 \times 10^{-5} < P < 4 \times 10^{-4}$ atm) were assumed to be controlled by a combination of vaporization and diffusion of the various species. Several combinations of the recession rates as calculated by Equations 2 and 13, were tried in an attempt to describe the rates in the intermediate pressure range. Of the equations tried, the following yielded the best correlation between experimental and

calculated rates:

$$\log(\dot{x}) = 24.030\ \log(\dot{x}_D) + 3.781(\log(\dot{x}_D))^2 + 0.193(\log(\dot{x}_D))^3$$
$$- 15.155\ \log(\dot{x}_v) - 2.548(\log(\dot{x}_v))^2 - 0.131(\log(\dot{x}_v))^3 + 15.762 \quad [14]$$

where $\dot{x}_D$ is the rate as calculated by Equation 2 and $\dot{x}_v$ is the rate as calculated by Equation 13. These equations used to describe the recession rates at the intermediate pressures were obtained by least-squares curvefitting with respect to the experimental recession rates in the intermediate pressure range.

A simple computer program was used to calculate recession rates at the experimental conditions, in both oxygen and air. The results are presented in Tables 10 and 11 in the appendix respectively. Curves representing the surface recession rate in oxygen and air for a wire 0.0559 cm in diameter are shown in Figures 3 and 4 respectively. The degree of correlation between experimental rates and rates calculated by Equation 14 is indicated in Table 8.

Table 8. Effectiveness of the Final Correlation for Rates in Oxygen at Pressures in the Intermediate Range ($3 \times 10^{-5} < P < 4 \times 10^{-4}$ atm)

Temp °C	Approximate Experimental Scatter, %	Correlation Disparity, %
1965	14.2	9.8
2110	25.1	32.0
2260	20.0	21.8
Overall	19.8	21.2

An indication of the correlation (over the pressure range of 9.8×10^{-8} to 1.32 atm) of the experimental and calculated rates in oxygen is presented in Table 9.

Table 9. Effectiveness of the Final Correlation for Oxidation in Oxygen

Temp °C	Approximate Experimental Scatter, %	Correlation Disparity, %
1965	7.8	9.1
2110	15.6	16.7
2260	15.8	17.3
Overall	12.8	14.2

CHAPTER VI

DISCUSSION OF RESULTS

Examination of Figures 3 and 4 revealed no visible differences in the oxidation behavior of the iridium wire from Lots 1, 2, and 3. This is substantiated numerically by Tables 10 and 11 in the appendix.

Examination of Figure 3, along with Tables 6, 7, 8, and 9, revealed that an effective correlation between the experimental and theoretical recession rates for oxidation in oxygen was achieved. As there were too few data points for oxidation in air, an analysis for the experimental scatter could not be performed. An examination of Figure 4 indicates that the correlation between the experimental and theoretical recession rates was effective.

When considering the uncertainty of $\pm$ 6.0 to 6.5 kcal/mole for work done by Norman *et al*, $\pm$ 0.9 kcal/mole for work done by Olivei, and $\pm$ 0.3 to 0.7 kcal/mole for the present studies, the free energies of formation for $IrO_3(g)$ agree fairly well. When considering the free energies of formation for $IrO_2(g)$, the disparity between the results of the present studies and the results of Norman *et al* is greater. Olivei reported no free energies of formation for $IrO_2(g)$. The results of Olivei and the present study, which have the lesser uncertainties, are in closest agreement.

CHAPTER VII

SUMMARY

There is quite good agreement between experimental and theoretical surface recession rates for oxidation in both oxygen and air. The theoretical rates were based upon empirical equations for the free energies of formation of the species involved in the oxidation process. The results of these empirical equations are also in quite good agreement with the results of previous investigators.

$Ir(g)$, $IrO_2(g)$, and $IrO_3(g)$ were thought to be the major species involved in the surface recession of the wire. At low pressures ($P < 3 \times 10^{-5}$ atm), the rate was assumed to be predominated by the vaporization of the various species. For high pressures ($P > 4 \times 10^{-4}$ atm), the rate was thought to be controlled by gaseous diffusion of the various species through a boundary layer. At the intermediate pressure ($3 \times 10^{-5} < P < 4 \times 10^{-4}$ atm), the rate was assumed to be controlled by a combination of vaporization and diffusion of the species.

CHAPTER VIII

SUGGESTIONS FOR FUTURE WORK

A search for a better equation describing the surface recession rate in the intermediate pressure range is in order. The equation at present (Equation 14) does not allow for a smooth transition over the entire pressure range. One possible equation that should be investigated is

$$\dot{x} = \frac{P - P_1}{P_2 - P_1} \dot{x}_D + \frac{P_2 - P}{P_2 - P_1} \dot{x}_v$$

where P_1 is the pressure at the upper limit of validity for Equation 13, P_2 is the lower limit of validity for Equation 2, $\dot{x}_D$ is the recession rate as calculated from Equation 2, and $\dot{x}_v$ is the recession rate as calculated by Equation 13. This type of equation forces a smooth transition over the entire pressure range but the quality of the fit of this equation with respect to the experimental data is unknown at present.

It should be kept in mind that this type of equation is the result of assuming that the recession rate in the intermediate pressure range is controlled by a combination of vaporization and gaseous diffusion.

REFERENCES

1. Cordefunke, E. H. P. and Meyer, G., "The System Iridium-Oxygen, I. Measurements of the Volatile Oxide of Iridium", Rec. Trav. Chim., 81, pp. 495-504, 1962.

2. Alcock, C. B. and Hooper, G. W., "Thermodynamics of the Gaseous Oxides of the Platinum Group Metals", Royal Society of London, Proceeding Series A, Vol. 254, pp. 551-61, 1960.

3. Schäfer, V. H. and Heitland, H. J., "Gleichgewichtsmessungen im System Iridium-Sauerstoff Gasförmiges Iridiumtrioxyd", Z. Anorg. Allgem. Chem., 304, pp. 249-65, 1960.

4. Norman, J. H., et al, "Mass Spectrometric Study of Gaseous Oxides of Iridium", Journal of Physical Chemistry, Vol. 42, pp. 1123-4, 1965.

5. Olivei, A., "Methods for Studying Oxygen-Platinum Metals Interaction", Journal of the Less Common Metals, Vol. 29, pp. 11-23, 1972.

6. Wimber, R. T. and Kraus, H. G., "Oxidation of Iridium", Metallurgical Transactions, July 1974.

7. Halvorson, J. and Wimber, R. T., "Thermal Expansion of Iridium at High Temperatures", Journal of Applied Physics, Vol. 43, pp. 2519-22, June 1972.

8. McLaren, E. H., Murdock, E. G., and Kirby, C. G. M., "A Method for the Control and Measurement of Wire Temperature in Preparatory Anneals on Standard Pt/Pt-10Rh Thermocouples", The Review of Scientific Instruments, Vol. 43, No. 5, pp. 827-8, May 1972.

9. Kraus, H. G., Natural Convection High Temperature Oxidation of Iridium, Master's Thesis, Montana State University, June 1973.

10. Honig, R. and Kramer, D. A., Techniques of Metals Research, Vol. IV, Part I, Interscience Publishers (John Wiley & Sons), New York, pp. 515-16, 1970.

11. Sherwood, T. K. and Pigford, R. L., Absorption and Extraction, McGraw-Hill, New York, pp. 91-2, 1952.

12. Hilsenrath, J., et al, Tables of Thermal Properties of Gases, NBS Circ. 564, 1955.

13. Rohsenow, W. M. and Harnett, J. P., Handbook of Heat Transfer, McGraw-Hill, New York, Section 2, pp. 84-5, 1973.

14. Dushman, S., Scientific Foundations of Vacuum Technique, John Wiley & Sons, New York, pp. 30, 1962.

15. Madden, A. J. and Piret, E. L., Proceedings of the General Discussion on Heat Transfer, Institution of Mech. Engrs. and Am. Soc. of Mech. Engrs., New York, pp. 328-33, 1951.

16. Drake, R. M., et al, "Free Convection Heat Transfer from Horizontal Cylinders to Gases at Transition Knudsen Numbers", Heat-Mass Transfer and Thermodynamics, pp. 119-132.

17. Emmert, R. E. and Pigford, R. L., "Gas Absorption and Solvent Extraction", Chemical Engineers Handbook, 4th Ed., R. H. Perry, et al, Edtrs., McGraw-Hill, New York, pp. 20-1, 1968.

18. Bell, W. E., Tagami, M., and Inyard, R. E., "Dissociation of Iridium Oxide", Journal of Physical Chemistry, Vol. 70, pp. 2048-50, 1966.

19. Cordefunke, E. H. P. and Meyer, G., Rec. Trav. Chim., Vol. 81, pp. 670-8, 1962.

20. Searcy, A. W., et al, Chemical and Mechanical Behavior of Inorganic Materials, Wiley-Interscience, New York, pp. 108-11, 1970.

21. McAdams, W. H., Heat Transmission, McGraw-Hill, New York, pp. 320, 1954.

APPENDIX

APPENDIX A

Table 10. Experimental Conditions and Experimental and Calculated Recession Rates for Oxygen

Run No.	Lot No.	Temp. (°C)	Press. (Torr)	Avg. Diam. (cm)	Experimental Rate (cm/sec)	Calculated Rate (cm/sec)
1*	1	1675	1.0E 00	0.0409	3.52E-07	3.10E-07
2*	1			0.0610	2.44E-07	2.42E-07
3*	2			0.0492	2.50E-07	2.77E-07
4*	2			0.0523	2.68E-07	2.67E-07
5*	1		1.0E 01	0.0616	5.70E-07	5.46E-07
6*	1			0.0640	5.35E-07	5.29E-07
7*	2			0.0465	6.29E-07	6.82E-07
8*	2			0.0498	6.58E-07	6.46E-07
9*	1		1.0E 02	0.0582	1.46E-06	1.58E-06
10*	1			0.0614	1.50E-06	1.51E-06
11*	2			0.0509	1.58E-06	1.74E-06
12*	2			0.0474	1.60E-06	1.84E-06
13*	1		1.0E 03	0.0522	6.34E-06	6.90E-06
14*	1			0.0615	5.89E-06	6.25E-06
15*	1			0.0567	6.51E-06	6.56E-06
16*	1			0.0516	7.28E-06	6.95E-06
17*	1			0.0463	8.15E-06	7.44E-06
18*	1			0.0401	9.38E-06	8.17E-06
19*	1			0.0574	7.84E-06	6.51E-06
20*	2			0.0506	7.07E-06	7.04E-06
21*	2	1820	1.0E 00	0.0497	4.53E-07	4.56E-07
22*	2			0.0521	4.25E-07	4.47E-07
23*	2			0.0463	4.96E-07	4.68E-07
24*	2		5.0E 01	0.0609	1.79E-06	1.83E-06
25*	2			0.0656	1.58E-06	1.73E-06
26*	2			0.0457	2.26E-06	2.28E-06
27*	2		1.0E 03	0.0428	9.56E-06	9.90E-06
28*	2			0.0464	9.32E-06	9.40E-06
29*	2			0.0494	1.01E-05	9.03E-06
30*	1	1965	7.5E-05	0.0609	9.47E-09	1.27E-08
31	2			0.0499	1.21E-08	1.27E-08
32	1			0.0563	1.13E-08	1.27E-08
33	2		5.0E-04	0.0459	1.60E-08	1.35E-08

Table 10 (continued)

Run No.	Lot No.	Temp. (°C)	Press. (Torr)	Avg. Diam. (cm)	Experimental Rate (cm/sec)	Calculated Rate (cm/sec)
34*	1	1965	5.0E-04	0.0616	1.12E-08	1.35E-08
35*	1			0.0569	1.11E-08	1.35E-08
36	2		1.0E-02	0.0495	3.12E-08	3.21E-08
37	2			0.0476	3.09E-08	3.21E-08
38	3			0.0496	3.41E-08	3.21E-08
39	2		5.0E-02	0.0477	6.51E-08	8.71E-08
40*	1			0.0618	9.80E-08	8.73E-08
41*	1			0.0652	7.73E-08	8.74E-08
42	2		1.0E-01	0.0500	1.55E-07	1.50E-07
43*	1			0.0538	1.53E-07	1.50E-07
44*	1			0.0502	1.57E-07	1.50E-07
45*	1		1.0E 00	0.0479	8.05E-07	7.62E-07
46*	1			0.0517	5.46E-07	7.43E-07
47*	1			0.0547	6.80E-07	7.28E-07
48*	2			0.0505	7.45E-07	7.49E-07
49*	2			0.0480	7.76E-07	7.62E-07
50*	1		1.0E 01	0.0455	2.61E-06	2.29E-06
51*	1			0.0552	2.15E-06	2.00E-06
52*	1			0.0638	1.62E-06	1.80E-06
53*	1			0.0600	1.76E-06	1.88E-06
54*	1			0.0583	1.97E-06	2.00E-06
55*	1			0.0519	2.13E-06	2.09E-06
56*	1			0.0489	2.57E-06	2.18E-06
57*	2			0.0518	2.30E-06	2.09E-06
58*	1		1.0E 02	0.0406	5.11E-06	5.05E-06
59*	1			0.0532	3.68E-06	4.12E-06
60*	2			0.0516	3.57E-06	4.21E-06
61*	2			0.0489	3.97E-06	4.39E-06
62*	1		1.0E 03	0.0604	1.07E-05	1.04E-05
63*	1			0.0634	9.48E-06	1.01E-05
64*	2			0.0504	1.19E-05	1.17E-05
65*	2			0.0463	1.27E-05	1.23E-05
66	2	2110	7.5E-05	0.0446	4.79E-08	1.04E-07
67	1			0.0517	1.06E-07	1.04E-07
68	3			0.0436	1.44E-07	1.04E-07
69	2		5.0E-04	0.0483	7.70E-08	1.06E-07
70	1			0.0318	9.80E-08	1.06E-07

Table 10 (continued)

Run No.	Lot No.	Temp. (°C)	Press. (Torr)	Avg. Diam. (cm)	Experimental Rate (cm/sec)	Calculated Rate (cm/sec)
71	2	2110	5.0E-04	0.0420	1.22E-07	1.06E-07
72	3		1.0E-02	0.0496	1.32E-07	1.37E-07
73	3			0.0503	1.32E-07	1.37E-07
74	1			0.0573	1.30E-07	1.37E-07
75+	2		5.0E-02	0.0489	2.58E-07	1.62E-07
76	2			0.0480	1.22E-07	1.62E-07
77	1			0.0604	1.90E-07	1.63E-07
78	2		1.0E-01	0.0482	4.26E-07	2.32E-07
79	2			0.0499	2.32E-07	2.33E-07
80	1			0.0630	2.17E-07	2.35E-07
81	3		1.0E 00	0.0483	1.22E-06	1.45E-06
82	3			0.0495	1.06E-06	1.43E-06
83*	2			0.0581	1.35E-06	1.35E-06
84*	2			0.0550	1.49E-06	1.38E-06
85*	2			0.0491	1.21E-06	1.44E-06
86*	2		5.0E 01	0.0625	4.81E-06	4.77E-06
87*	2			0.0569	5.09E-06	5.12E-06
88*	2			0.0513	6.05E-06	5.54E-06
89*	2		1.0E 03	0.0626	1.29E-05	1.44E-05
90*	2			0.0583	1.50E-05	1.51E-05
91*	2			0.0540	1.58E-05	1.58E-05
92	3	2260	7.5E-05	0.0471	7.49E-07	7.15E-07
93	2			0.0488	6.24E-07	7.15E-07
94*	1			0.0564	3.47E-07	7.15E-07
95*	1			0.0650	6.66E-07	7.15E-07
96	2		5.0E-04	0.0468	6.59E-07	7.17E-07
97	1			0.0621	3.87E-07	7.17E-07
98*	1			0.0605	5.15E-07	7.17E-07
99*	1			0.0586	2.66E-07	7.17E-07
100	3		1.0E-02	0.0452	8.56E-07	7.73E-07
101	3			0.0465	8.12E-07	7.73E-07
102	1			0.0603	7.75E-07	7.73E-07
103*	1		5.0E-02	0.0521	7.81E-07	5.85E-07
104*	1			0.0529	4.54E-07	5.85E-07
105*	1			0.0651	7.74E-07	5.86E-07
106*	1		1.0E-01	0.0572	8.81E-07	6.91E-07
107*	1			0.0522	7.28E-07	6.90E-07
108*	1			0.0613	5.30E-07	6.92E-07
109*	1			0.0517	6.35E-07	6.90E-07

Table 10 (continued)

Run No.	Lot No.	Temp. (°C)	Press. (Torr)	Avg. Diam. (cm)	Experimental Rate (cm/sec)	Calculated Rate (cm/sec)
110*	1	2260	1.0E 00	0.0544	1.49E-06	1.87E-06
111*	1			0.0561	1.67E-06	1.85E-06
112*	1			0.0644	1.93E-06	1.79E-06
113*	1			0.0584	1.83E-06	1.84E-06
114*	2			0.0481	1.96E-06	1.92E-06
115*	2			0.0481	2.40E-06	1.92E-06
116*	1		1.0E 01	0.0564	5.83E-06	5.74E-06
117*	1			0.0567	5.33E-06	5.72E-06
118*	2			0.0501	5.61E-06	6.19E-06
119*	2			0.0463	6.30E-06	6.50E-06
120*	1		1.0E 02	0.0488	1.32E-05	1.24E-05
121*	1			0.0494	6.84E-06	1.23E-05
122*	1			0.0597	6.52E-06	1.07E-05
123*	2			0.0516	8.73E-06	1.19E-05
124*	2			0.0513	1.08E-05	1.19E-05
125*	1		1.0E 03	0.0475	3.59E-05	2.87E-05
126*	1			0.0639	2.20E-05	2.38E-05
127*	2			0.0478	2.82E-05	2.78E-05
128*	2			0.0416	3.29E-05	3.14E-05

* denotes runs performed by Kraus (9)

\+ denotes the run represented in Figure 2

NOTE: Computer notation of 7.50E-05 corresponds to either 7.50×10^{-5} Torr or 7.50×10^{-5} cm/sec.

APPENDIX B

Table 11. Experimental Conditions and Experimental and Calculated Recession Rates for Air

Run No.	Lot No.	Temp. (°C)	Press. (Torr)	Avg. Diam. (cm)	Experimental Rate (cm/sec)	Calculated Rate (cm/sec)
1	3	1675	5.0E-01	0.0462	3.12E-08	4.05E-08
2	3		5.0E 00	0.0500	9.63E-08	8.61E-08
3	3			0.0498	7.90E-08	8.64E-08
4	3		5.0E 01	0.0496	1.73E-07	1.75E-07
5	3		5.0E 02	0.0481	6.05E-07	5.28E-07
6	3			0.0493	5.28E-07	5.19E-07
7	2	1965	7.5E-05	0.0469	1.71E-08	1.26E-08
8	2		5.0E-04	0.0495	9.67E-09	1.28E-08
9	2		1.0E-02	0.0508	1.35E-08	1.67E-08
10	2			0.0493	1.02E-08	1.67E-08
11	2		7.5E-02	0.0499	6.80E-08	3.50E-08
12	3			0.0478	3.32E-08	3.50E-08
13	2		5.0E-01	0.0509	1.07E-07	1.06E-07
14	2		5.0E 00	0.0505	3.38E-07	3.44E-07
15	2			0.0502	3.32E-07	3.46E-07
16	2		5.0E 01	0.0473	5.51E-07	6.55E-07
17	2			0.0458	6.65E-07	6.72E-07
18	2		5.0E 02	0.0502	1.22E-06	1.24E-06
19	2			0.0502	1.12E-06	1.24E-06
20	2	2260	7.5E-05	0.0474	5.35E-07	7.14E-07
21	2			0.0461	8.62E-07	7.14E-07
22	2		5.0E-04	0.0475	8.26E-07	7.15E-07
23	3			0.0481	6.61E-07	7.15E-07
24	3			0.0480	7.88E-07	7.15E-07
25	2		1.0E-02	0.0502	7.30E-07	7.27E-07
26	2		7.5E-02	0.0491	8.55E-07	4.77E-07
27	2		5.0E-01	0.0485	6.85E-07	4.73E-07
28	2			0.0449	6.94E-07	4.78E-07
29	1		5.0E 00	0.0566	9.52E-07	1.01E-06
30	2			0.0489	9.66E-07	1.10E-06
31	2			0.0463	1.03E-06	1.13E-06
32	2		5.0E 01	0.0491	1.63E-06	1.98E-06
33	1			0.0602	1.29E-06	1.70E-06
34	2		5.0E 02	0.0499	2.87E-06	3.50E-06
35	1			0.0618	2.57E-06	3.03E-06

Wahl, Neil Kelly

Natural-convective high-temperature oxidation of iridium.

[redacted]